3D ESTIMATION OF SLOW GROUND MOTION USING INSAR AND THE SLOPE ASPECT ASSUMPTION, A CASE STUDY: THE PUNCAK PASS LANDSLIDE, INDONESIA

N. H. Isya[1,2,*], W. Niemeier[1], M. Gerke[1]

[1] Technische Universität Braunschweig, Institute of Geodesy and Photogrammetry, Germany - (n.isya, w.niemeier, m.gerke)@tu-bs.de
[2] Institut Teknologi Sepuluh Nopember, Dept. of Geomatic Engineering, Indonesia

KEY WORDS: InSAR, 3D components, LOS, slope movement, downward motion

ABSTRACT:

The Indonesian Centre of Volcanology and Geological Hazard Mitigation classified the Ciloto district as one of the most landslide prone areas in Indonesia. Some evidence of ground movement and the landslide failures occurred in recent years. Thus, continuous monitoring is necessary for supporting the precautions of an upcoming landslide. This study applies Small Baselines - Slowly Decorrelated Phase Filter (SDPF) for InSAR processing both for the ascending and the descending data. The primary objective is to generate horizontal and vertical components of InSAR results from two different tracks and slope aspect information in order to retrieve a projection to the northward direction. We used the available Sentinel-1 SAR data from 2014 until 2018. Combination of two orbits is approached by the surface and the nearest-neighbor gridding method. The 3D components were examined at the Puncak Pass, Ciloto, an active landslide area. For the case study area, it appeared that soil materials transferred slowly from the top of main body landslide to the accumulated zone near to the buildings owned by a local resort. The cumulative 3D displacements for three years were computed for the depleted zone: it moved -47, 23, -10 mm for dU, dE and dN, respectively. Meanwhile, the accumulated zone was considered having the up-lift motion to maximum 43, -13, 7 mm, respectively.

1. INTRODUCTION

Interferometric Synthetic Aperture Radar is very well established for measuring the earth's surface changes from spaceborne in recent years. A considerable number of research studies have identified seismic activities such as the impact of earthquakes (Funning et al., 2005), the behavior of volcanoes (Liu et al., 2015), and the slow movement in prone landslide areas (Cascini et al., 2014). The Permanent Scatter (PS) (Ferretti et al., 2001) and SBAS technique (Berardino et al., 2002) are advanced DInSAR methods to generate the real deformation and reduce unwanted signals coming from orbit and topographic errors, atmospheric effects, and noise. Hooper et al. (2007) determined the character of those unwanted signals utilizing the amplitude and the phase analysis. Those phases of interferograms are correlated spatially, which are; the signal associated with the isolated movement of individual brightness considered as noise, the variation in atmospheric delay between two acquisitions, the orbital errors in azimuth, and the residual orbit error term in range due to a consequence of interferometric processing. Moreover, the look angle error is also partly spatially correlated. Thus, the estimation of spatial correlation for the four terms and part of the fifth term could be subtracted from the interferograms.

Landslides have a complex behavior of movement which is challenging to determine the geometry of unstable surface due to the lack of real-time (in-situ) observation. One effective technique to observe the surface's motion, in general, is the radar remote sensing. The InSAR time series examination is highly recommended to comprehend Ciloto landslide's behavior. However, one of the limitations of this technology is that the interferometric phase is observed in the slant range direction. This geometry leads to the displacement result in the line of sight (LOS) projection. Therefore, a combination of several different geometries is needed to generate three vector components. Two independent observation from different tracks data could fulfill this requirement and determine two vectors, the vertical and the east-west direction (Ferretti, 2014). Because the satellite orbit is close to the polar direction, it makes the detection of deformation insensitive to the north-south-component. To overcome this problem, we assume that in case of landslide studies, the deformation will point downhill.

This paper describes the process and result of generating the 3D field of slow displacements both from the ascending and the descending InSAR data under the assumption that the horizontal component has a motion parallel to the downhill slope. We applied our method specifically in the Puncak Pass region. The result shows evidence of slow deformation for three years, where in February and March 2018, two consecutive landslides occurred within the area. We investigated the cumulative movement geometrically using our 3D slope aspect method for three years. Notably, we quantified motion in the depleted and accumulated zones.

2. STUDY AREA AND DATA

PVMBG[1] classified the Ciloto district, West Java as one of the most landslide prone areas in Indonesia since in recent years there were the ground movement and landslides occurred in this region. The Ciloto landslide zone is located from the hilly ridge to creek valley. The CiJember river flows in the middle of this area. The slope is mostly about 15^{o} - 25^{o} and in some parts there are steep slopes about 50^{o} facing south-east direction. The highest and lowest altitudes are 1530 and 1175 m above MSL, respectively, with the distance between those altitudes about 2.6 km. This mountainous area was built to residence and agriculture.

*Corresponding author

[1] Centre of Volcanology and Geological Hazard Mitigation

This contribution has been peer-reviewed. The double-blind peer-review was conducted on the basis of the full paper.
https://doi.org/10.5194/isprs-annals-IV-2-W5-623-2019 | © Authors 2019. CC BY 4.0 License.

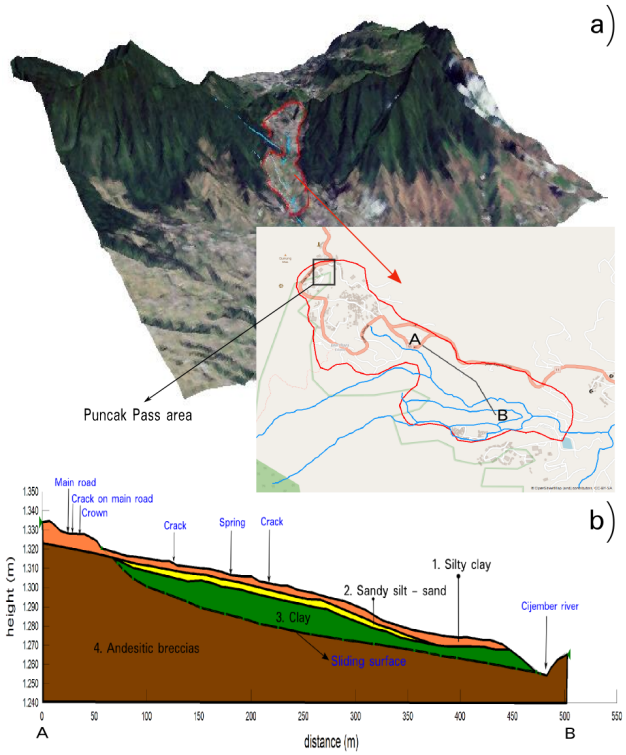

Figure 1. a) The study area is located in the Ciloto District, West Java, Indonesia. The 3D map describes the hilly area along the CiJember river flowing in the middle of it. b) The drilling profile based on line A-B in Fig 1.a.

According to the geologic map of West Java, the primary type of rock around Ciloto is Quaternary volcanic rocks consisting of basalt, andesitic tuffs especially breccia, and lava from local vents (Limo Mountain). Based on a previous geological survey in the middle of the study area (Sumaryono et al., 2015), the bore drilling result identified the layers as seen on the drilling profile in Figure 1.b, which are; (1) Silty clay from the surface to 3 m depth; (2) Sandy silt - sand in 3-7 m depth; (3) Clay with the thickness about 1 m; (4) Andesitic breccias in 8-11 m depth. The silty clay mostly covered the top layer followed by the sandy silt - sand layer. A sliding surface laid between clay and andesitic breccias layer. Since the geological form belonged to volcanic rocks, this layer was quite stable in conditions where no great saturated water was infiltrated into the ground. However, upon these volcanic rocks, there was a reposed clay layer having the water content of 51% and cohesion of 0.1 kg/cm^2. This laboratory result gave a substantiation why the border layer was easily sliding to the lower elevation.

The Puncak Pass

The Puncak Pass locates at the top of the study area classified by PVMBG as the highest potential ground movement class. This phenomenon mainly occurs due to high precipitation that affected surface and groundwater volumes. Based on the geological report, clay and sand (weathering soil) with brown to red-brown color was found at the upper part of the Puncak Pass in 1-5 m depth. Meanwhile, the lower part was composed of igneous rocks, primarily breccias (identified as the layer of slip surface) and a mix of sand and clay. These forms are vulnerable to move if the abundance of surface and groundwater is not flowing properly. Moreover, an old movement which occurred in 2014 on the location could be re-activated and stimulate the slope instability.

Two Puncak Pass landslides occurred on Sunday, 4th February and Wednesday, 28th March 2018 after heavy rainfall events. It was located at 6^o 42' 27" S and 106^o 59' 38" E, 1450 - 1500 m above MSL near to the Puncak Pass resort hotel. The landslide had 60^o gradient slope with the toe's part about 10^o. PVMBG categorized them into a type of debris slide. The landslide's geometry, for the length, width, and depth from crown to the main body, was 59 m, 50 m, and 25 m, respectively. The landslide's materials moved to the southern direction (N 182^o E). The total length from the debris' source to the toe of surface rupture was 101 m. Several factors causing these landslides are; a very steep slope ($\geq$ 45^o), strongly porous weathered soil, the weak shear strain due to weathering and water infiltration, a bad drainage system, and high rainfall intensity as the main trigger factor.

Concerning this event, an investigation is necessary to understand the slow movement's behavior quantitatively before these two successive landslides occurred in early 2018. Such information would help to comprehend whether particular motions occurred before the actual failure's event. Thus, a continuous geodetic observation might help to identify possible slope failures in a similar environment and support the precautions. The InSAR technique is one of the solutions to quantify surface changes both in horizontal and vertical directions especially for a motivation to figure out depleted and accumulated landslide's zones.

2.1 Data

We processed large archive SAR data from Sentinel-1 A/B both the ascending track (72 SAR images with the relative orbit number = 98) and the descending track (68 SAR images with the relative orbit number = 47) starting from October 2014 until June 2018. The Digital Elevation Model (DEM) from SRTM 1 arc-second was used in purpose to reduce the topography effect on SAR processing and generate the slope aspect information.

3. METHODS

3.1 Small Baselines Interferograms

We generated the interferograms in full resolution using GMTSAR (Sandwell et al., 2011) and modified the pre-processor steps being suitable to the STAMPS format (Hooper, 2008). For the SAR pre-processing, the SLCs images were convoluted by the Gauss 5x5 kernel in order to create the amplitude and preserve the spatial relationship between the pixels. Furthermore, we calibrated each image by a weighting factor calculated from the ratio between the amplitude of each SAR image and the mean amplitude for a whole set of images (Lyons and Sandwell, 2003). We then calculated the amplitude difference dispersion with the same algorithm from Ferretti et al. (2001) and Hooper (2008) as an indication of phase stability using the ratio between the mean amplitude of all master-slave pairs and the standard deviation of the difference amplitude. This selection of phase stability candidates was performed to reduce a big computational process for many master-slave configurations.

After generating the interferograms controlled by 150 m spatial and 150 days temporal baseline for both the ascending and the descending SAR data, we applied Small Baselines (SBAS) with Slowly Decorrelating Filter Phase (SDFP) algorithm for the time series InSAR analysis. The algorithm defined by phase characteristics has the main purpose of identifying Persistent Scatter (PS)

alike the single master configuration (Hooper et al., 2007). However, it uses the bandpass filtering of surrounding pixels to estimate the spatially-correlated contribution to the interferometric phase for the small baselines networks. Furthermore, the final unwrapping phase results have also been corrected by the power-law tropospheric delay explained in our previous work (Isya et al., 2018).

3.2 The Slope Aspect

The availability of Sentinel-1 both for ascending and descending at across-track view allows estimating 2D displacement vectors regarding vertical and east-west motions. However, retrieving the 3D deformation components is still challenging for a small rate movement's study because of an insensitivity to observe at along-track direction. Hence, the inversion model to estimate the third component needs, at least, one independent observation incorporating from another geodetic data source such as GNSS (Global Navigation Satellite System) (Polcari et al., 2016) or Ground-based Radar (Carl et al., 2018) measurement. Another possibility is to assume the characteristics of displacement whose geometric information is available as a priority (Hu et al., 2014). For the slope movement case, the motion takes into account as its direction towards the aspect of downslope considering a natural characteristic of a geophysical phenomenon. This assumption was applied to the monitoring of ice-sheet motion (Joughin et al., 1998; Meyer, 2003). We also assume for the landslide's motion in the Ciloto having a slope-parallel surface. The north-south motion is suggested as a projection from the west-east component using the angle from the estimated slope aspect as shown in Figure 2.b. The projection only concerns the direction of movement and computes the scalar result as a *pseudo* component.

In the beginning, we interpolated the InSAR results in time for the further time series analysis. Since PS scatters from the ascending and the descending orbit have different geometric locations, the first step was that we tried to relocate both results using either the surface (Smith and Wessel, 1990) or the nearest-neighbor (Ebdon, 1985) gridding method. The surface function interpolates the irregular space (x,y,z) data to be gridded using *the adjustable tension continuous curvature splines*. The algorithm is an improvement of the minimum-curvature surface (Swain, 1976) that is commonly used in the earth sciences for the gridding method. Meanwhile, the nearest-neighbor function assigns an average value to each node which has at least one or more PS points within a radius centered on the node. The average value is calculated as a weighted mean of the nearest PS point from each sector inside the search radius (Wessel et al., 2019).

The gridded table data produced by the surface function were masked by the location of amplitude difference dispersion (ADD) (x,y) to control the possibility of distorted interpolation on the non-value pixels location. On the other hand, if we used the nearest-neighbor method, the gridded outcome created new resampled pixels at a certain radius (30 m for this case). Finally, we selected them with a criterion having a pixel value both from the ascending and the descending data process. Consequently, the number of LOS pixels generated by the surface method was higher than from the nearest-neighbor method.

The next step was estimating vertical (dU) and horizontal (dE, dN) components using a Gauss-Markov model or linear regression analysis. We firstly computed local incidence angles and heading angles based on a master SAR scene used by the earlier co-registration process. The slope aspects were computed from

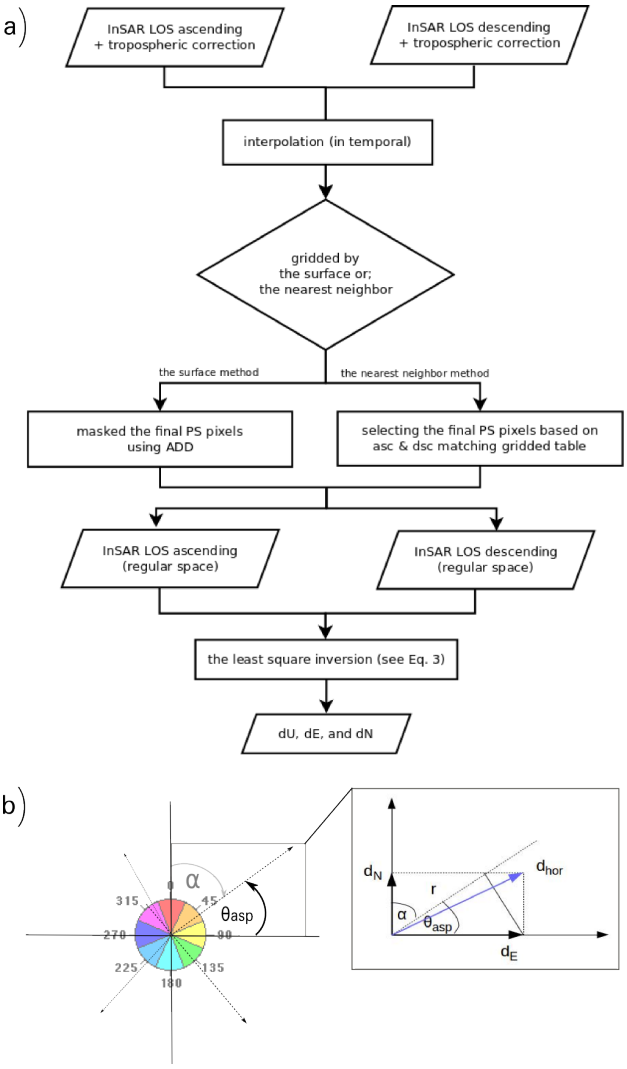

Figure 2. a) The strategy to estimate 3D vector displacements using the different tracks of InSAR data and the slope aspect. b) The assumption of northern component as a result from eastern vector projected by aspect information

the DEM (i.e., SRTM 30 m) using an algorithm that incorporates the values of the cell's eight neighbors (Burrough and McDonell, 1998). The slope aspect pixels were resampled spatially in purpose to similize the registered LOS grids.

Regarding the projection from LOS to ground looking geometry, the 3D vector displacement is approached by an original least square (OLS) estimator. The matrix design in Eq. (3) for the first and second rows are generated from decomposition of the displacement vector projected to one slant-range component both viewed by ascending and descending direction (Hanssen, 2001). Meanwhile, the third row is supposed to the characteristic of landslide movement in a hilly area. Because we assumed the northern component having a motion parallel to down-slope direction, we projected the eastward to northward vector employing the slope aspect as the third equation derived by,

$$d_N = r \cdot cos(90 - \theta_{asp}) \quad (1)$$

with,

$$r = d_E \cdot cos(\theta_{asp}) \quad (2)$$

where θ_{asp} is the slope aspect angle, d_N and d_E are northern and

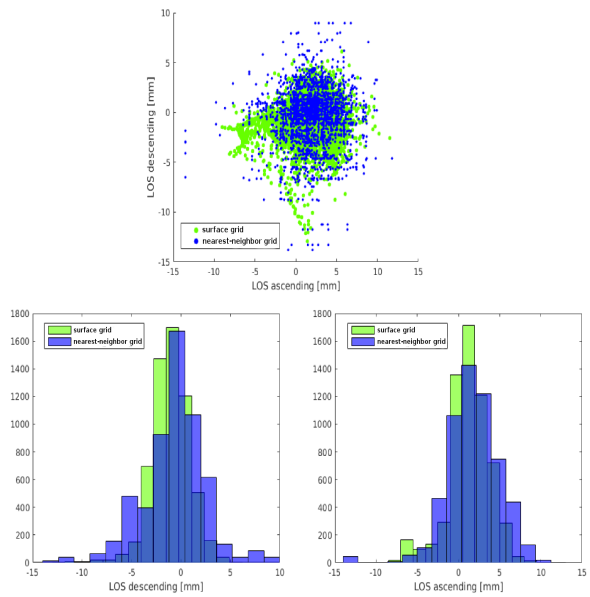

Figure 3. The top image shows a scatter distribution between the nearest-neighbor and the surface merging result while the bottom images show the histogram both for the ascending and the descending data. The sample of scatters was captured on the bottom part of Ciloto District. The sample PS points are located in a stable urban area near to the Ciloto district (ca. 9 km2 area's size).

eastern component, respectively and r is the related projection vector between d_N and d_E.

Furthermore, we estimated d_U, d_E, and d_N using the least square inversion as described in the following equation

$$\begin{bmatrix} cos(\theta_{inc_{asc}}) & -sin(\theta_{inc_{asc}})\ sin(\alpha_{h_{asc}}) & sin(\theta_{inc_{asc}})\ cos(\alpha_{h_{asc}}) \\ cos(\theta_{inc_{dsc}}) & -sin(\theta_{inc_{dsc}})\ sin(\alpha_{h_{dsc}}) & sin(\theta_{inc_{dsc}})\ cos(\alpha_{h_{dsc}}) \\ 0 & cos(\theta_{asp})\ cos(90-\theta_{asp}) & -1 \end{bmatrix} \cdot \begin{bmatrix} d_U \\ d_E \\ d_N \end{bmatrix} = \begin{bmatrix} d_{LOS_{asc}} \\ d_{LOS_{dsc}} \\ 0 \end{bmatrix} \tag{3}$$

where θ_{inc} is the incidence angle and α_h is the satellite platform heading angle - $3\pi/2$.

4. RESULTS AND DISCUSSION

4.1 3D Generation in The Ciloto District

We estimated 3D vectors displacement generated by two tracks InSAR data under the slope aspect assumption without any external data from ground measurements since the area was lack of up-to-date geodetic survey information. The combination of two orbits SAR data was assessed both by the surface and the nearest-neighbor method. Figure 3 shows the scatters comparison between these methods. The number of PS points differs between the methods. For a whole region of interest that we used in the computation, the number of scatters found from the surface method is 2.15 times larger than that of the nearest-neighbor method.

Based on Varnes (1978), the detected deformation is classified as a creep that moves slowly and continuously to downslope. Soil

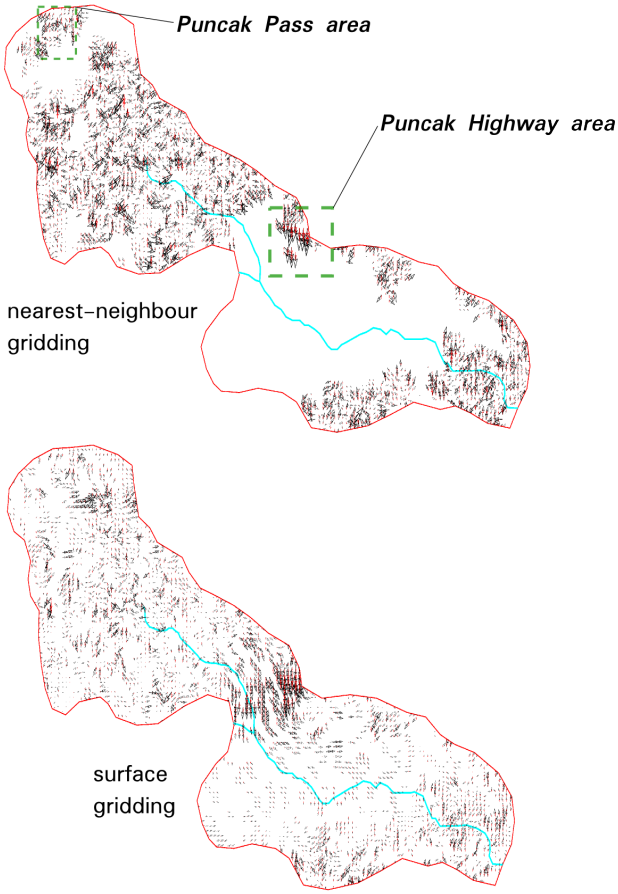

Figure 4. The gridded result from nearest-neighbour (the top image) and surface method (the bottom image). The black arrow represents the horizontal component and the red one for vertical component. The cyan lines illustrates the Cijember river.

and rocks sustained by either seasonal or continuous creep are not completely classified as a landslide, but they perform a significant role in the slow displacement of the landslide blocks (Terzaghi and of America , GSA) as a potential factor for increasing the shear stress periodically. Van Asch (1984) distinguished two phases in a landslide; (a) the phase of initial failure, and (b) the subsequent phase after movement has started and the mass material runs out (Brunsden and Thornes, 1979). Because slow creep movements could precede the initial failure of a slope, the following analysis focuses on the rate of displacement and velocity progressively.

In general, we defined a 3D displacement field for horizontal and vertical movements in the Puncak Pass, Ciloto as illustrated in Figure 4. The previous investigation from Supriatna (2002) explained that the main trigger of movement was the increasing of water intensity caused by rainfall and water infiltration. Considering that the rate of InSAR displacement accelerates progressively, the potential ground movement could occur at the Puncak Pass, the residents at the south-east Puncak Pass (RW.06) and Puncak-Bogor Highway.

The Puncak Pass Landslide Two samples in Puncak Pass area were collected to comprehend the behavior of slope movement. The zone (1) and (2) are located on the top near to the main road and the bottom close to the Puncak Pass resort & hotel, respectively. Figure 5 represents the mean LOS time series InSAR result from both the ascending and the descending data. An unwrapping

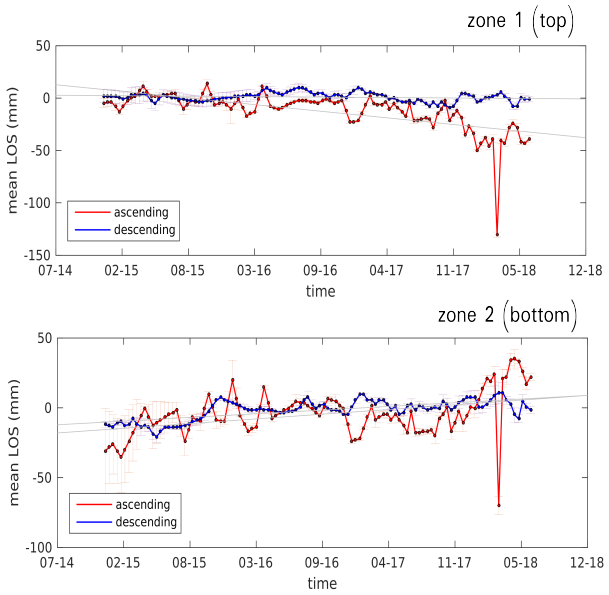

Figure 5. The mean LOS InSAR result both the ascending and the descending data in the Puncak Pass area.

error was detected close to the landslide events in February and March 2018. We applied the correction of one phase unwrapping error introduced by Notti et al. (2015). Since the differential displacement between two consecutive acquisitions (residue) from the ascending data at the surface failure's events exceeded $|\lambda/4|$ x 2 mm, we could not correct the error easily. Hence, we assumed this range time as a breakpoint due to largely displaced materials. In order to highlight the great motion occurred in this period, the time series graphs were modified to be $residue \pm \lambda$. Furthermore, the trend of displacement generated by the ascending data identifies more significant deformation signals than descending data because the area has a slope facing east-southern direction (130^o - 160^o for the slope aspect).

We assessed the generated 3D vectors displacement specifically in the Puncak Pass landslide. A sufficient number of PS points was found at the location because persistent objects existed there. Those are the road, permanent buildings owned by a resort hotel, local houses, and natural objects such as rocks and trunks. The temporal displacements were calculated using the time series inversion technique (Schmidt and Buergmann, 2003) producing LOS displacements and subsequently projecting those to the vertical (dU) and the horizontal (dE,dN) motions. A surface model is used further to grid the table of vertical time series displacements as a visual interpretation whereas the horizontal component is plotted by the velocity vector ($\overrightarrow{dE}$,$\overrightarrow{dN}$). Figure 6. b describes the cumulative vertical and horizontal displacement and identifies the top of the Puncak Pass as a crown landslide's body considering clear evidence of pre-failure surface. The head of the landslide's body cumulatively moved down -5 cm in vertical and 1-2 cm in horizontal from November 2014 to January 2018. For a typical creep movement, there might be a definite location where it was going to deposit. We found a streak of fragment assumed as the landslide deposit (expected as a landslide's toe) at the southeast part. Meanwhile, the horizontal vectors show that their directions are parallel to downslope towards the southeast. Considering the east-westward perspective (the original dE generation from retrieving the 2D inversion of two tracks InSAR data), the vectors agree to aspect's direction where the top of landslide's body had motions toward the east and partly west while the middle of that moved to eastward and for the bottom area toward the west. In particular, the result evaluates that the landslide began from the very slow movement (1-2 cm/year) and increased significantly to rapid movements close to the failure's events. Therefore, there was a possibility at certain places where a high rate movement might exist, but we could not identify on the SAR signal because of the decorrelation (e.g., a rapid change of amplitude value).

PVMBG documented the Puncak Pass landslides and assessed the aftermath. The crown body was placed at Cianjur-Bogor Street and moved to the western hall of Puncak Pass resort (a red arrow in Fig. 6a). The estimated vertical motion given by Sentinel-1 data shows a slowly subside to -5 - -10 cm in general. Due to a lack of distributed PS points on the whole sub-area, the horizontal vector is not precisely conducting a direct path direction to the scarp deposit but tends to move both from the south-west and the south-east direction at the top landslide's body. In the middle part, we could see an uplift displacement proving that the materials moved toward south-eastern, even though PS points were not available between the change of vertical motion (down - uplift or the red and blue scale color). The line profile (black color) presents the main body and material deposit for 25 m and 76.2 m, respectively. We compared a line profile (purple color) from the InSAR observation which the result is slightly different to the field survey, 45 m for the zone of depletion (see number 1 from Fig. 6b) and 80 m for the zone of accumulation (see number 2). Close to the toe of the surface of rupture, the PVMBG's investigation found the ponded water indicating a slip surface spot. It weakened the shear strength since there was direct contact between the layer of weathering soil (sand and clay materials) and a waterproof curtain.

Regarding the retrieving 3D motion field, we realize that the third element comes from an assumption of slope aspect derived by a high model. If the source of DEM has a low-middle resolution, the downslope direction to its neighbors might not be computed precisely. We used SRTM 1 arc-second (30 meters) as a DEM source which was still reliable to describe the finest pixel resolution of the slope aspect regarding the size of the area (170 x 220 m). Another issue is that PS points are not distributed homogeneously in the whole observed area. Considering the motion beginning from the head of main scarp to the foot part and ending at the toe, we partly dissolve the direction flow of surface failure whether straightly moved to southern part N 182^o E (a red arrow on Fig. 6a) or started from north-west at the main body then went to south-east for the zone of accumulation. The reason for this uncertain direction is that the slow movement derived by InSAR data has a more variate direction than the report described by the PVMBG on 6^{th} April 2018.

Additionally, another investigation to the previous landslide (4^{th} February 2018) occurred at the same location gives a more understandable description of the western part of the landslide's body. The preceding report explained that they found a crack at the hotel's hall located in the north-west area (Fig. 6b) with the length ca. 5 m toward south-east N 145-148^o E. It confirms that the ground movement in this area moved both from the north-west and north-east to south-east region. Moreover, a spring (the blue dot in Fig. 6a) was found as well at the south-east part of the sub-area. Hence, a potential of follow-up landslides in the future might occur if there are no proper precautions to prevent the surface's failure.

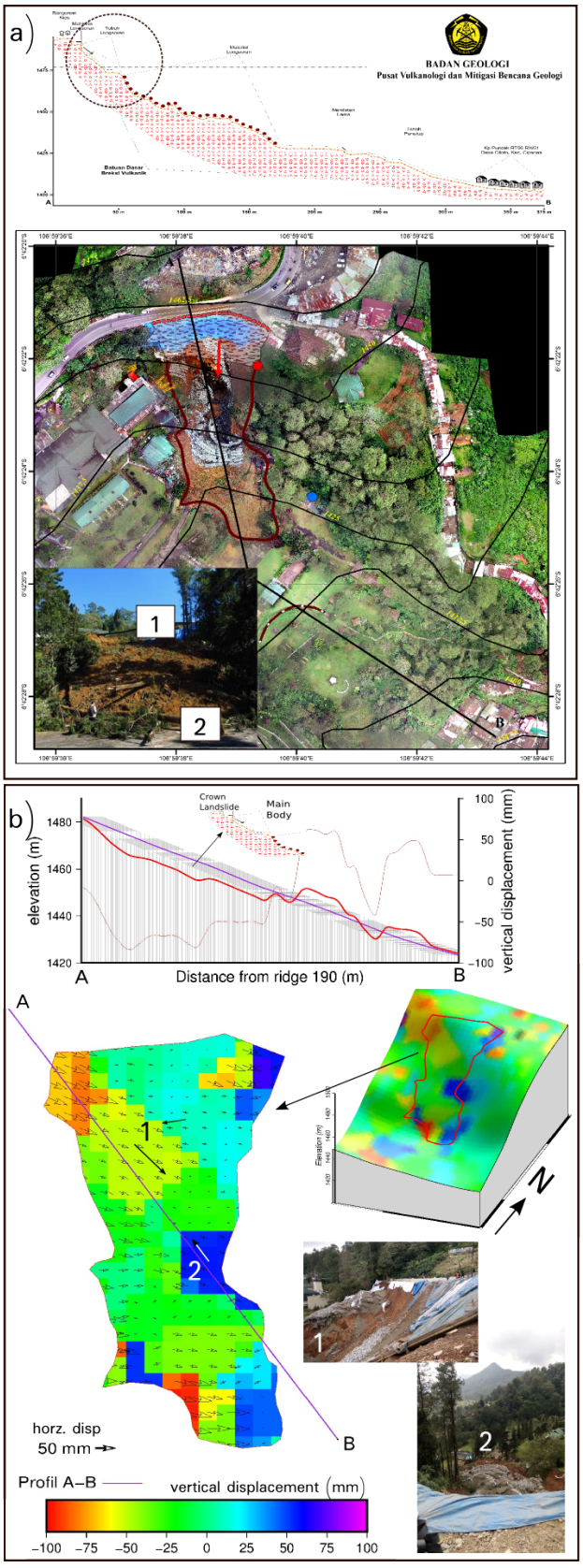

Figure 6. a) An aerial photography after the landslide, on 28th March 2018 occurred. b) The 3D motion field generated by the InSAR from November 2014 to January 2018. The pictures show a profile of the cumulative vertical displacement occurred at the Puncak Pass which the horizontal displacement moved from the road to the lower surface's elevation placed a few buildings owned by a resort hotel.

4.2 Relationship between 3D Vectors Displacement and Precipitation

The heavy rainfall intensity and bad drainage system caused the pond water flowing along a slide surface as seen in Figure 6. b. It infiltrated to porous soil and accumulated among the space of grains and cracks. Since soil contains saturated water, it makes the mass weight and pore pressure increases while the shear strength decreases. Because of the possible impact of rainfall to motion's behavior, a relationship between precipitation and slope movement is necessary to be further investigated.

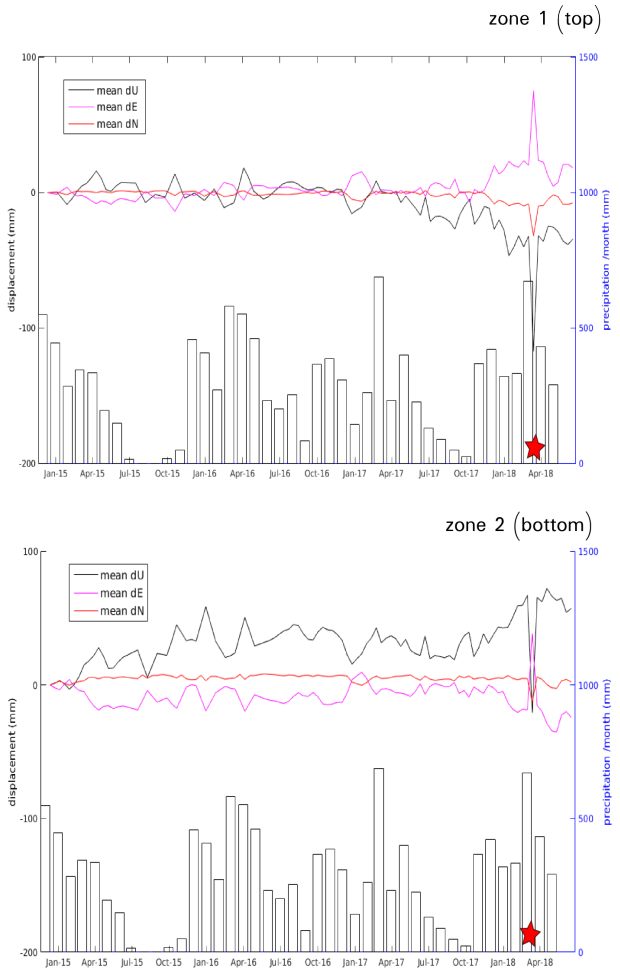

Figure 7. InSAR displacements in U, E, N directions at zone of depletion (1) and zone of accumulation (2) in the Puncak Pass landslide along with the total precipitation (/month). The red star indicates the date of two consecutive landslides occurred in February and March 2018. The correlation values between displacement vectors and precipitation are -0.04, 0.25, -0.22 (zone 1) and 0.22, -0.07, -0.2 (zone 2).

3D vectors samples at zone 1 determined as the depletion area with 18 PS scatters [-6.706° - -6.705° S; 106.993° - 106.994° E]) are compared to the total precipitation (per month [mm]) recorded by the Citeko Station. The total rainfall intensities recorded from October 2016 to February 2017 for five months (rainy season) was 1788 mm with the highest intensity in February 2017, 688.5 mm. Figure 7 (top) shows that all vectors within this time indicate maximum cumulative motion to -47 mm, 23 mm, -10 mm for dU, dE and dN, respectively. Additionally,

a significant movement also occurred from December 2014 - September 2015. The vertical components denote upwards in the rainy season (December - February) while during the dry season (March - September), they point downwards. The other geological behavior might influence on this final result because the surface soil material containing clay tends to expand during the wet season (expansive clay) and otherwise shrinks on the dry season called as creep phenomenon. In total, we observed a slow motion towards downslope with the mean velocity of -10±9, 5±5, -2±2 mm/year for dU, dE and dN, respectively and its rates increasingly to cm/day close to the debris slide's event. In that case, the SAR sensor was not able anymore to detect the rapid movement due to a limit of phase sensitivity. The RMSEs (root mean square errors) are relatively high since the model fit to calculate the mean velocity (mm/year) is using the linear regression. The model, however, does not account for non-linear behavior caused by precipitation and a hydrology factor. Therefore, a non-linear model fitting is better to be used in the future for predicting the displacement trend and velocity.

The graph for 20 PS scatters at zone 2 [-6.7065° - -6.7063° S; 106.9941° - 106.9943° E] located at the southern zone of accumulation is shown in Figure 7 (bottom). The cumulative displacements (dU, dE, dN) until 12th January 2018 are 43, -13, 7 mm, respectively. The samples are taken near to a building owned by the Puncak Pass hotel with the direction motion slightly towards the south-west. The mean velocities assumed as a linear displacement rate for dU, dE, dN are 10±12, -1±8, -0.2±2 mm/year, respectively. The significant acceleration has started since February 2017. The early period (December 2014 - January 2017) of time series displacement results is relatively stable. The indication of an oscillation pattern might also take into account if we consider the influence of rainfall intensity on the slope movement's characteristic. Although this zone suffered from low coherent objects, the generated 3D vectors indicate that the vertical component moved to up-lift describing the simultaneous ground movement displaced slowly from the top to downhill. Meanwhile, it is still difficult to determine the accurate horizontal direction in this zone because of the heterogeneity of rate velocities on the dE and dN component through the observed period. The linear regression does not fit the trend velocity as well demonstrated by very low coefficient of determination ($R^2 d_U$ = 0.4266, $R^2 d_E$ = 0.0181, $R^2 d_N$ = 0.0114).

We calculated a linear correlation between the rainfall intensity, recorded at the local station 6.5 km away, and the detected displacement in the Puncak Pass region. We approached both precipitation and total displacement cumulative values on each month to simplify the relationship pattern. The correlation in depleted zone (1) shows R_{d_U} = -0.04, R_{d_E} = 0.25, R_{d_N} = -0.22 while in accumulated zone (2) shows R_{d_U} = 0.22, R_{d_E} = -0.07, R_{d_N} = -0.2. The correlation values indicate that the precipitation is not a constantly main trigger factor for the slope movement. However, close to the landslide's events in February and March 2018, there were significant movements in both zones since February 2017 with the correlation rising R_{d_U} = 0.293, R_{d_E} = 0.072, R_{d_N} = -0.043 and R_{d_U} = 0.395, R_{d_E} = -0.248, R_{d_N} = 0.288, respectively. The motion relates to the increase of precipitation chat bars especially on the rainy season (November 2017 - March 2018) which the highest second record of precipitation proves the slope failure occurred on the area and makes the time series trend having an unwrapped error due to an insensitivity for detecting large deformation at small region and short time, namely, during the failure event. This interception is considered as a breakpoint shown by the red star in Figure 7.

5. CONCLUSIONS

We evaluated the slow movement's behavior in the 3D vectors displacement and tested the time series deformed signal to the real event landslide's location. Several ground movements observed in the Ciloto district, considered as the highest threatened area for landslide hazard, are classified as the extremely slow - slow rate displacement (several mm/year) known as creeps. However, the motion rate was simultaneously moving faster to cm or m unit close to slope's failure event. This type of movement resulted in the two successive Puncak Pass landslides occurred in February and March 2018. The second landslide was a debris slide with its moderate size of landslide about 60 x 170 m. We did not find out a direct linear relationship to the recorded rainfall intensity. Nevertheless, there was a strong indication of rainfall influence from November 2017 until March 2018. The Puncak Pass area constantly moved in this range of time.

Two approaches combining PSs from the ascending and the descending data are the nearest-neighbor and the surface gridding method. We evaluated both methods in this case study, but the nearest-neighbor function mostly created the final results. The nearest-neighbor gridding method might lose some well-detected signals if the matched location of a registered grid is only found on one track data. The surface method could avoid the loss of good candidate scatters caused by the adjustable interpolation from its neighbor. Nonetheless, the control of the final matching procedure might still have a bias since its parameter is taken by the amplitude dispersion index (ADI) either from the ascending or the descending data. Hence, we suggest applying the R-Index computation (Notti et al., 2014) to choose correctly which orbit's direction is the best to observe the slope geometry.

The method to generate 3D vectors is using two independent InSAR look directions under the slope aspect assumption. The north-south vector is calculated as a projection from the east-west component utilizing the angle of slope aspect. The slope assumption only works for a motion parallel to down-slope direction. Even for landslide studies, the surface of rupture might be more complicated to be illustrated only based on the slope aspect generated by DEM. The landslide might occur not only on a planar but also a circular slide surface. It might be better that the third assumption is based on a local characteristic of a landslide, such as the mechanism of soil movement, and considers a local geophysical survey.

ACKNOWLEDGEMENTS

The SAR data are provided by Open Access Copernicus, European Space Agency (ESA). We would like to thank BPBD[2] Cianjur and PVMBG to give a guide and detail explanation about the Ciloto Landslide. The research is supported by Deutscher Akademischer Austauschdienst (DAAD).

References

Berardino, P., Fornaro, G., Lanari, R. and Sansosti, E., 2002. A new algorithm for surface deformation monitoring based on small baseline differential sar interferograms. *IEEE Transactions on Geoscience and Remote Sensing* 40(11), pp. 2375–2383.

[2]Regional Disaster Management Authority

Brunsden, D. and Thornes, J. B., 1979. Landscape sensitivity and change. *Transactions of the Institute of British Geographers* 4(4), pp. 463–484.

Burrough, P. A. and McDonell, R. A., 1998. *Principles of Geographical Information Systems*. Oxford University Press, New York.

Carl, T., Farina, P., Intrieri, E., Ketizmen, H. and Casagli, N., 2018. Integration of ground-based radar and satellite insar data for the analysis of an unexpected slope failure in an open-pit mine. *Engineering Geology* 235, pp. 39 – 52.

Cascini, L., Calvello, M. and Grimaldi, G. M., 2014. Displacement trends of slow-moving landslides: Classification and forecasting. *Journal of Mountain Science* 11(3), pp. 592–606.

Ebdon, D., 1985. *Statistics in Geography*. Blackwell.

Ferretti, A., 2014. *Satellite InSAR Data. Reservoir Monitoring from Space*. European Association of Geoscientist and Engineers.

Ferretti, A., Prati, C. and Rocca, F., 2001. Permanent scatterers in sar interferometry. *IEEE Transactions on Geoscience and Remote Sensing* 39(1), pp. 8–20.

Funning, G. J., Parsons, B., Wright, T. J., Jackson, J. A. and Fielding, E. J., 2005. Surface displacements and source parameters of the 2003 bam (iran) earthquake from envisat advanced synthetic aperture radar imagery. *Journal of Geophysical Research: Solid Earth*.

Hanssen, R., 2001. *Radar Interferometry: Data Interpretation and Error Analysis*. Remote Sensing and Digital Image Processing, Springer Netherlands.

Hooper, A., 2008. A multi-temporal insar method incorporating both persistent scatterer and small baseline approaches. *Geophysical Research Letters* 35(16), pp. n/a–n/a. L16302.

Hooper, A., Segall, P. and Zebker, H., 2007. Persistent scatterer interferometric synthetic aperture radar for crustal deformation analysis, with application to volcn alcedo, galpagos. *Journal of Geophysical Research: Solid Earth* 112(B7), pp. n/a–n/a. B07407.

Hu, J., Li, Z., Ding, X., Zhu, J., Zhang, L. and Sun, Q., 2014. Resolving three-dimensional surface displacements from insar measurements: A review. *Earth-Science Reviews* 133, pp. 1 – 17.

Isya, N. H., Riedel, A., Riedel, B. and Niemeier, W., 2018. Comparison of power law tropospheric correction for time series insar application. In: *Wissenschaftlich-Technische Jahrestagung der DGPF und PFGK18 Tagung in Mnchen*, Deutschen Gesellschaft fr Photogrammetrie,Fernerkundung und Geoinformation e.V., pp. 483 – 507.

Joughin, I. R., Kwok, R. and Fahnestock, M. A., 1998. Interferometric estimation of three-dimensional ice-flow using ascending and descending passes. *IEEE Transactions on Geoscience and Remote Sensing* 36(1), pp. 25–37.

Liu, P., Li, Q., Li, Z., Hoey, T., Liu, Y. and Wang, C., 2015. Land subsidence over oilfields in the yellow river delta. *Remote Sensing* 7(2), pp. 1540–1564.

Lyons, S. and Sandwell, D., 2003. Fault creep along the southern san andreas from interferometric synthetic aperture radar, permanent scatterers, and stacking. *Journal of Geophysical Research: Solid Earth*.

Meyer, F. J., 2003. Simultane Schaetzung von Topographie und Dynamik polarer Gletscher aus multi-temporalen SAR Interferogrammen. PhD thesis, Institut fuer Photogrammetrie und Kartographie, Technische Universitaet Muenchen.

Notti, D., Calò, F., Cigna, F., Manunta, M., Herrera, G., Berti, M., Meisina, C., Tapete, D. and Zucca, F., 2015. A user-oriented methodology for dinsar time series analysis and interpretation: Landslides and subsidence case studies. *Pure and Applied Geophysics* 172(11), pp. 3081–3105.

Notti, D., Herrera, G., Bianchini, S., Meisina, C., Garca-Davalillo, J. C. and Zucca, F., 2014. A methodology for improving landslide psi data analysis. *International Journal of Remote Sensing* 35(6), pp. 2186–2214.

Polcari, M., Palano, M., Fernndez, J., Samsonov, S. V., Stramondo, S. and Zerbini, S., 2016. 3d displacement field retrieved by integrating sentinel-1 insar and gps data: the 2014 south napa earthquake. *European Journal of Remote Sensing* 49(1), pp. 1–13.

Sandwell, D., Mellors, R., Tong, X., Wei, M. and Wessel, P., 2011. Gmtsar: An insar processing system based on generic mapping toolsgmtsar: An insar processing system based on generic mapping tools. Technical report, Scripps Institution of Oceanography.

Schmidt, D. A. and Buergmann, R., 2003. Time-dependent land uplift and subsidence in the santa clara valley, california, from a large interferometric synthetic aperture radar data set. *Journal of Geophysical Research: Solid Earth* 108(B9), pp. n/a–n/a. 2416.

Smith, W. H. F. and Wessel, P., 1990. Gridding with continuous curvature splines in tension. *Geophysics* 55(3), pp. 293–305.

Sumaryono, S. T., Sulaiman, C., Triana, Y. D., Robiana, R. and Irawan, W., 2015. *Landslide Investigation and Monitoring at Ciloto, West Java, Indonesia*. Springer International Publishing, Cham, pp. 1089–1096.

Supriatna, A., 2002. Kajian spasial gerakan tanah di kp. baru, desa ciloto, kab. cianjur. Master's thesis, Department of Geodetic Engineering, Bandung Institute of Technology.

Swain, C. J., 1976. A fortran iv program for interpolating irregularly space data using the difference equations for minimum curvature. *Coumputers and Geosciences* 1, pp. 231–240.

Terzaghi, K. and of America (GSA), G. S., 1950. *Mechanism of Landslides*. Harvard University, Department of Engineering.

Van Asch, T. W. J., 1984. Creep processes in landslides. *Earth Surface Processes and Landforms* 9(6), pp. 573–583.

Varnes, D. J., 1978. *Slope movement types and processes*. Vol. In Special Report 176: Landslides: Analysis and control, Transportation and Road research board, National Academy of Science, Washington D.C., chapter 2, pp. 11–33.

Wessel, P., Smith, W., Scharroo, R., Luis, J. and Wobbe, F., 2019. The Generic Mapping tools (GMT) Man Pages. Release 5.4.5.

APPENDIX

3D vectors displacement is computed by PS DISP. It is a bundled script written on bash shell and Matlab code. The script requires GMT and Matlab Software and can be downloaded on https://github.com/dedetmix/PS_DISP.